Analysis of dephasing signal in picosecond stimulated-Raman-gain experiments

Martine De Mazière,* Chris Sierens,† and Dirk Schoemaker

Department of Physics, University of Antwerp, B-2610, Wilrijk-Antwerpen, Belgium

Received February 24, 1989; accepted June 28, 1989

A detailed theoretical analysis is presented of the dephasing signal measured in four-beam picosecond time-resolved stimulated-Raman-gain experiments. The analytical expressions derived are successful in simulating observations on the CS_2 model system under various experimental conditions. It is established that the tail of the curve for sufficiently long delay times is uniquely determined by the vibrational Raman term that yields the vibrational dephasing time T_2. It is also found that the rotational dephasing time cannot be fundamentally determined from the rotational Raman peak centered around zero delay. Furthermore, it is shown that the coherence properties of the stimulating laser fields, as distinguished from their pure pulse-envelope properties, are crucially important in determining the time resolution of the experiments and for explaining several experimental phenomena observed under mismatched excitation-pulse conditions. In this respect, the domain model for mode-locked pulses has proved to be useful. It is found that the time resolution of the dephasing measurements is determined by the combined pulse-coherence time of the driving fields and not by the cross-correlation width of the pulse envelopes.

1. INTRODUCTION

Several laser-spectroscopic techniques with picosecond time resolution have been developed for studying the relaxation of excitations in condensed matter.[1–6] One distinguishes energy- and phase-relaxation mechanisms, which are characterized by the times T_1 and T_2, respectively.[2–6] For the excitations that are probed in the experiment, one aims at determining the relaxational time constants as well as the decay mechanisms and decay channels. To this end, the coherent nonlinear Raman techniques have proved powerful.[2,4–6] In particular, the time-resolved coherent anti-Stokes Raman scattering (CARS) technique has been explored.[5–8]

The feasibility of four-beam time-resolved stimulated-Raman-gain (TR SRG) spectroscopy was demonstrated by Heritage.[9] However, an in-depth analysis of the dephasing signal that is measured in such experiments is still lacking. Only recently[10,11] has a way for improving the initial incomplete analysis[9] been indicated, but it has not been carried out explicitly. Moreover, artifactual effects induced by the stimulating laser pulses have been noted, e.g., in CARS experiments.[7,12,13] These also have not yet been examined sufficiently in depth.

In view of the foregoing, we have performed a complete analysis of the TR SRG dephasing signal directly in the time domain. The theoretical description encompasses several terms in the total signal that originate in the various degrees of freedom that are intrinsic to the sample. The convolution with the characteristics of the laser fields is taken into account explicitly.

We have made detailed tests of our theory by analyzing picosecond Raman-gain dephasing data on the 656- and 992-cm^{-1} vibrational modes in the liquids CS_2 and C_6H_6, respectively. Various experimental conditions have been studied; in particular, both the timing mismatch within each laser pair and the tunings of both laser frequencies relative to each other have been varied. Thereby, additional questions have arisen concerning the characteristics of the dephasing signal, in particular those near zero-delay time.

Our starting expression, approximations, and notation are given in Section 2. The relevant parameters are introduced in Section 3: The experimental ones reflect our typical experimental circumstances and technique (Subsection 3.A), and the intrinsic ones are modeled according to the Born–Oppenheimer approximation (Subsection 3.B). The latter are connected with known spectroscopic data. The various signal contributions are identified correspondingly.

A discussion of some general symmetry properties of the signal is presented in Subsection 4.A. However, for comparison with experiment a specific pulse model must be chosen. With a simple Gaussian pulse-envelope model (Subsection 4.B.1) we cannot obtain agreement with all the observations of Subsection 4.B.2. Agreement, however, is reached after we introduce the domain model[14,15] for the (extrinsic) pulse parameters (Subsection 4.B.3). The resulting analytical expressions for the dephasing signal are numerically evaluated (Subsection 4.C), and this makes it clear that we are able to simulate the experiments satisfactorily (see Subsection 4.D). Also, the important subject of time resolution is addressed.

Although the analyses are carried out with regard to our specific four-beam TR SRG setup, their extension to different polarization, modulation, or geometrical configurations is straightforward.

2. BASIC EXPRESSIONS FOR THE TIME-RESOLVED SRG SIGNAL

The dephasing information in a TR SRG experiment is contained in the time evolution of the third-order nonlinear polarization $\mathbf{P}^{(3)}$.

The four-beam setup,[16] a simplified presentation of which is shown in Fig. 1, makes use of a pair of laser pump pulse trains and a delayed replica pair of probe pulse trains. The subscripts L and S refer to the pump fields at the higher (ω_L)

0740-3224/89/122376-16$02.00

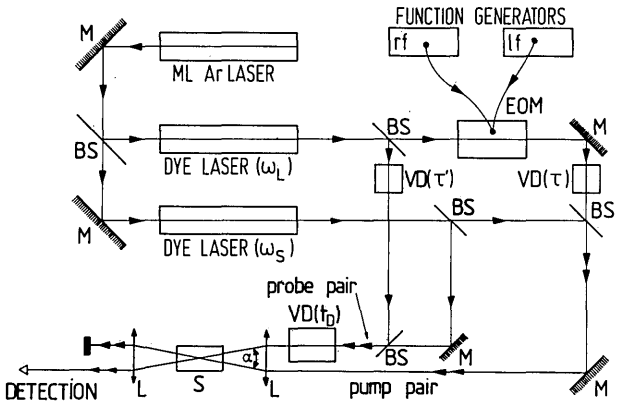

Fig. 1. Schematic presentation of the four-beam TR SRG setup for the measurement of Raman dephasing times, using the double-modulation technique of Ref. 16: BS's, beam splitters; EOM, electro-optic modulator; VD's variable delays; M's, mirrors; L's, lenses; S, sample. The rms value of the dephasing signal $\mathcal{S}(t_D)$ is measured.

and lower (Stokes, ω_S) frequencies, respectively (angular frequencies are used throughout this paper), and L' and S' to the corresponding probe replicas at the same frequencies; $\mathbf{k}_{L(S)}$ and $\mathbf{k}_{L'(S')}$ are their respective wave vectors. The frequency difference $(\omega_L - \omega_S)$ is tuned to resonance with the Raman vibration at frequency Ω_R in the sample. An eventual deviation from the resonance condition will be indicated by δ_R:

$$\delta_R = \Omega_R - (\omega_L - \omega_S). \tag{1}$$

For the dephasing signal $\mathcal{S}$, we effectively select the Stokes component of $\mathbf{P}^{(3)}$ that is responsible for the gain on the Stokes probe amplitude $E_{S'}$, namely, $\mathbf{P}^{(3)}_{S'}$; its wave vector is $\mathbf{k}_P$. It is well established[10] that in a heterodyne detection configuration the signal $\mathcal{S}$ is given by:

$$\mathcal{S} = -\frac{\omega_S}{2T}\,\mathrm{Im}\left\{\int_0^T dt E^*_{S'}(t)\int_0^l dx P^{(3)}_{S'}(x,t)\exp[i(k_P - k_{S'})x]\right\}. \tag{2}$$

It is an average over a pulse-train period T.

The slowly varying quasi-monochromatic plane-wave approximation has been made, together with the assumption of quasi-collinear propagation along x. The (x, t) frame is the retarded one[5,6] that propagates along with the pulses (along x) at the common group velocity v. Color dispersion of v between ω_L and ω_S is neglected.

In the cw mode-locked experiments that we consider, the small-gain limit[9] holds, and only the terms linear in the gain have been withheld in Eq. (2). Thus the apparent (complex) pulse-envelope amplitudes $E_{L(S)}(t)$ and $E_{L'(S')}(t)$ are the initial ones, and hence they are independent of the distance x traveled through the interaction length l.

Section 3 explicates $P^{(3)}_{S'}(t)$ and, consequently, the dependence of the dephasing signal $\mathcal{S}$ on the intrinsic sample and extrinsic experimental parameters.

3. FORMAL PARAMETERIZATION OF THE TR SRG-SIGNAL EXPRESSION

Integral expressions for the dephasing signal $\mathcal{S}(t_D)$, which for presentational purposes are gathered in Appendix A, are obtained after substituting into Eq. (2) the timing sequence of the exciting and probing laser pulses and a model for the time-dependent response of the medium. The variable t_D represents the delay between the two pairs of laser pulses. Our experimental conditions are taken into account. The development of our theoretical analysis is based on the assumption of a mutually parallel polarization of all stimulating laser fields—hence the omission of polarization subscripts throughout—and a response model suitable for liquids. Indeed, liquid CS_2 and C_6H_6 have functioned as experimental test samples because of the existence of extensive knowledge about their properties.

A. Incorporation of Experimental and Pulse-Sequence Parameters

Because neither laser depletion nor sample saturation needs to be considered, any x dependence in Eq. (2) occurs only through the wave-vector mismatch factor. This factor differs from 1 because pump and probe pairs cross each other in the sample under a small angle α. But, more importantly, it depends on which combination of laser fields is effectively driving the sample excitation. Therefore the experimental geometry influences the relative weight of the various signal contributions.

The integrated wave-vector mismatch factor,

$$M(\Delta\mathbf{k}) \equiv \int_0^l dx \exp[i(k_P - k_{S'})x], \tag{3}$$

is treated in an approximate way by estimating the effective mismatch $|\Delta\mathbf{k}|$:

$$|\Delta\mathbf{k}| = (\mathbf{k}_P - \mathbf{k}_{S'})\mathbf{k}_{S'}/|\mathbf{k}_{S'}| \tag{4}$$

and by accordingly associating a weight factor $m(\Delta\mathbf{k})$ to it:

$$m(\Delta\mathbf{k}) = \frac{\sin(|\Delta\mathbf{k}|l/2)}{|\Delta\mathbf{k}|l/2}\,l = |M(\Delta\mathbf{k})|. \tag{5}$$

The phase of $M(\Delta\mathbf{k})$ [Eq. (3)] will turn out to be irrelevant (Subsection 4.B.3).

In our experiments, the crossing angle $\alpha \sim 0.2$ rad, and $l \sim 0.2$ mm.[17] One should realize that a wrong estimate of l also changes the mutual ratios of the mismatch factors. Any other corrections for the departure from collinearity in practice are neglected in our theoretical analysis.

The mutual time relations among the four laser pulse trains are expressed as follows (see Fig. 1):

E_L stands for

$$E_L(t - \tau - t_{0,L})\exp[-i\omega_L(t - \tau - t_{0,L})]\exp(i\phi_L),$$

$E_{L'}$ stands for

$$E_{L'}(t - t_D - \tau' - t_{0,L})\exp[-i\omega_L(t - t_D - \tau' - t_{0,L})]\exp(i\phi_{L'}),$$

E_S stands for

$$E_S(t - t_{0,S})\exp[-i\omega_S(t - t_{0,S})]\exp(i\phi_S),$$

$E_{S'}$ stands for

$$E_{S'}(t - t_D - t_{0,S})\exp[-i\omega_S(t - t_D - t_{0,S})]\exp(i\phi_{S'}). \tag{6}$$

The envelope functions $E_{L'}$ and E_L are identical, and so are the ones for E_S and $E_{S'}$, but the primes are retained as an aid in distinguishing between the pump and probe character and for indicating a possible attenuation of the probe relative to the pump replica. In our experiments, the pump-to-probe intensity ratio was approximately 3 to 1.

Generally, the time delay t_D between both (ω_L, ω_S) pairs is chosen as the functional variable for $\mathcal{S}(t_D)$ (Appendix A). The time-mismatch parameters τ and τ' describe a possible deviation from synchronous overlap within the pair of pump and probe pulses, respectively.

Time jitter between both dye lasers[18] can be expressed through uncertainties in the time origins $t_{0,L}$ and $t_{0,S}$. Evidently, only the difference $\Gamma = t_{0,L} - t_{0,S}$ is relevant. The incorporation of a fixed value of Γ into the integral expressions of Appendix A is equivalent to substitution by $(\tau + \Gamma)$ and $(\tau' + \Gamma)$, respectively, for τ and τ'.

The carrier phases $\phi_{L(S)}$ and $\phi_{L'(S')}$ are set off because it is assumed that they are constants during a pulse. Following our double-phase-modulation-detection technique,[16,17] only ϕ_L carries a double [radio-frequency (a 10-MHz sine) plus low-frequency (a 15-Hz ramp)] modulation (see Fig. 1). Both modulations are slow compared with the pulse-repetition frequency (82 MHz). As a consequence, the initial equivalence between pump and probe fields of the same frequency (apart from their timing and direction of incidence or wave vector) is broken. Moreover, this detection scheme limits the signal to contributions that are modulated synchronously with ϕ_L. Therefore our selection of the field combinations that effectively add to $P_S^{(3)}$ in the integral expressions of the measured dephasing signal $\mathcal{S}(t_D)$ presented in Appendix A is made accordingly.

The integration limits have been extended to infinity because the experimental ratio of pulse-train period to pulse duration is $\sim 10^3$.

B. Medium Response Contributions to the TR SRG Signal

The classification of the various contributions to the dephasing signal $\mathcal{S}(t_D)$ in Appendix A is based on the Born–Oppenheimer approximation to the third-order nonlinear response function $X^{(3)}(\tau_1, \tau_2, \tau_3)$ of an isotropic medium[19]:

$$X^{(3)}(\tau_1, \tau_2, \tau_3) \propto \tfrac{1}{2}\sigma\delta(\tau_1)\delta(\tau_1 - \tau_2)\delta(\tau_2 - \tau_3) + \delta(\tau_1)d(\tau_1 - \tau_2)\delta(\tau_2 - \tau_3). \quad (7)$$

Here, the first term represents the electronic nonlinearities through an instantaneous δ-functionlike response (proportional to σ) and the second term describes the noninstantaneous nuclear response, through the behavior of $d(t)$. The latter specification to $d_{OR}(t)$, in $s_{OR,0}$ and $s_{OR,1}$, or to $d_R(t)$, in $s_{R,0}$ to $s_{R,3}$, refers to the orientational (OR) or vibrational (R) degrees of freedom.

Similarly, four two-photon-absorption contributions exist[17] that are resonant at the $(\omega_L + \omega_S)$ frequency. They are known to be relatively weak in CS_2 ($\sim 10^{-3}$) and to decay rapidly ($\sim 3 \times 10^{-3}$ psec).[20,21] We have presumed[17] a similar behavior in the case of C_6H_6. Therefore these terms are systematically neglected throughout.

Our identifications of the various terms in Appendix A, namely, two electronic terms ($s_{\sigma,0}$, $s_{\sigma,1}$), two orientational Raman terms ($s_{OR,0}$, $s_{OR,1}$), and four vibrational Raman terms ($s_{R,0}$ to $s_{R,3}$), will be used throughout this paper.

According to Ref. 10 and experimental evidence, an exponentially damped harmonic oscillation is attributed to the nuclear response function $d(t)$:

$$d(t) = d\,\frac{1}{T}\,1(t)\exp(-t/T)\sin[\cos](\Omega t), \quad (8)$$

where $1(t)$ symbolizes the unit step function.

The parameters to be determined, d for strength, T for relaxation time, and Ω for angular frequency, are labeled by the subscripts R and OR; the latter resides at near-zero frequency ($\Omega_{OR} \to 0$).

Real parameters d and T are preserved if in Eq. (8) a sine function is taken for the vibrational motion and a cosine function for the orientational one. Thereby one agrees with the continuity requirement for the system excitation at $t = 0$ and the requirements spelled out in Ref. 22.

Through Fourier transformation of the response function [Eq. (8)], the parameters are associated with experimental observables in frequency-domain spectroscopy.[10,17,19] In particular, the electronic response corresponds to a real frequency-independent susceptibility σ, and the nuclear response [Eq. (8)] to a Lorentzian of FWHM $2/2\pi T$, centered at $\Omega/2\pi$.

The nuclear-response parameters may be associated with the corresponding Raman cross sections.[21,22] From experimental data,[19,22–25] a consistent set of parameter values and, from that, relative scaling factors have been deduced; for CS_2, which we will discuss exclusively in this paper, they are, with respect to the 656-cm^{-1} mode ($d_R = 1$):

$$d_{OR} = 0.30,$$
$$\sigma = 0.062,$$
$$T_2 = 20 \text{ psec},$$
$$T_{OR} = 1.5 \text{ psec}. \quad (9)$$

4. DISCUSSION OF TR SRG SIGNAL CHARACTERISTICS

A. Properties Independent of a Specific Laser-Pulse Model

The integral expressions in Appendix A for the various contributions to the TR SRG signal $\mathcal{S}(t_D)$ reveal general properties that are independent of which specific laser-pulse model is chosen. We list the most important ones below.

First, one recognizes the occurrence of so-called coherent-coupling effects originating from interferences between two overlapping (in time and space) replicas of a same coherent laser field in, e.g., the electronic (s_σ) and orientational (s_{OR}) contributions. An extensive discussion is given in Subsection 4.D.2.

Second, for both instantaneous (s_σ) as well as for both orientational (s_{OR}) contributions, the signal generated at delay time t_D under mismatch conditions (τ, τ') is identical to its complex conjugate at $(-t_D)$ and (τ', τ) conditions. In the case when $\tau = \tau' = 0$, this symmetry property reduces to complete symmetry near the zero-delay time of its absolute magnitude. In addition, several coincidences among the different signal contributions can be recognized at the par-

ticular delay points $t_D = \tau - \tau'$ and $t_D = 0$.[17] (See Subsection 4.D.2.)

Third, with regard to the pulse sequence, it is evident that only the relative temporal mismatch between the ω_L and ω_S pulses within one pair is relevant.

A fourth property relates to the phase dependences of the various terms. For insensitivity to phase instabilities, an AC voltmeter lock-in detection technique is used,[16] by which the detected signal is essentially the rms value of the total sum $\mathcal{S}(t_D)$. Through this operation of squaring, however, a sum of product terms adds to the sum of all single, squared terms. But only the product of terms that have the same dependence on random phase instabilities needs to be considered: the sum of these terms, which is not explicated here, is called the mixing or interference term $\mathcal{T}$. The other product terms tend to zero average because they are liable to have phase noise.[16] The squared signal thus displays normally hidden information for the detection of which specific experiments have been designed.[20,21,24,26]

The effect of this interference term is shown explicitly in the signal simulations presented in Subsections 4.D.3 and 4.D.4. It is generally not negligible. From here on, the total signal—$\mathcal{T}$ included—will still be denoted by $\mathcal{S}(t_D)$.

B. Analytical Development of Separate TR SRG Terms after Inclusion of a Specific Laser-Pulse Model

1. *Analysis Based on a Gaussian, Frequency-Chirped Pulse*

The most natural first choice of a laser-pulse model is that of a Gaussian pulse envelope, of intensity widths $t_{p,L}$ and $t_{p,S}$ for ω_L and ω_S pulses, respectively. The possible occurrence of a linear frequency chirp is included through the parameters β_L and β_S. They lead to a spectral broadening by a factor $[1 + \beta_{L(S)}^2]^{1/2}$ (Ref. 27) and are negative or positive for linear upchirp or downchirp, respectively.

Specifically, one writes

$$E_L(t)\exp(-i\omega_L t) = \sqrt{I_L}\exp\left(-\frac{a_L}{2}t^2\right)\exp\left[-i\left(\omega_L t - \frac{a_L}{2}\beta_L t^2\right)\right], \quad (10a)$$

with

$$a_L = \frac{4\ln 2}{t_{p,L}^2}, \quad (10b)$$

and analogously for $E_S(t)$. Note that $E_{L(S)}(t)$ is a complex envelope amplitude.

After integration of the expression in Appendix A and taking into account Eq. (8), the analytical expressions obtained for the various contributions to the TR SRG signal are limiting cases of the ones derived in Subsection 4.B.3. Therefore they are not listed explicitly[17] here.

We restrict the discussion to the case of zero frequency chirp ($\beta_L = \beta_S = 0$), zero jitter ($\Gamma = 0$), zero resonance detuning ($\delta_R = 0$), and zero orientational frequency ($\Omega_{OR} = 0$). The spatial-mismatch factors are neglected temporarily because the terms are considered separately. The resulting simplified expressions are listed in Appendix B, and we comment on them briefly.

First, a common time-mismatch dependence, f_0, of Gaussian shape

$$f_0(\tau, \tau') = \exp\{-[(a_L a_S)/2(a_L + a_S)](\tau^2 + \tau'^2)\} \quad (11)$$

stands out, just as in our starting expressions. It is dominated by the largest of both pulse widths. Apart from this factor, some contributions, among which is $s_{R,0}$, stay intact as long as $\tau \equiv \tau'$.

Second, it is striking that among the vibrational Raman contributions only the $s_{R,0}$ term asymptotically reaches the expected exponential decay with characteristic relaxation time T_2. All other contributions fall off to zero following a dominant negative exponential quadratic in the delay t_D. In other words, the relaxational behavior for long delay times is dominated by the $s_{R,0}$ contribution. Therefore from here on we shall call $s_{R,0}$ the main Raman term.

Third, the buildup of the vibrational Raman terms near the zero-delay time is governed by the real complementary error function, erfc. More precisely, the error function's influence stretches roughly over the range where its argument changes from +1 to −1, giving to the exponentials in front weights that grow from 0 to 2. In particular, for the main Raman term in a normal, matched situation ($\tau = \tau' = 0$), this range is

$$-\frac{1}{\sqrt{C_0}T_2} + \frac{1}{2C_0T_2^2} \le \frac{t_D}{T_2} \le \frac{1}{\sqrt{C_0}T_2} + \frac{1}{2C_0T_2^2}, \quad (12a)$$

with

$$C_0 = (a_L + a_S)/4. \quad (12b)$$

It reflects the convolution between sample and excitation-pulse characteristics. The delay of the peak position of the signal and the possibility of determining T_2 are set by the ratios of pulse durations a_L and a_S to T_2. Thus the important question of time resolution is encountered. It is examined in more detail in Subsection 4.D.5.

Fourth, in addition to the second and third points above, it is clear that the behavior of the signal near zero delay is determined by the sum of all contributions. Thus the slow buildup of the main Raman signal is hidden under the superposition of the other zero-delay peaks. Because of the sensitivity of these contributions to all relevant parameters, their detailed structure will be discussed below.

At this point we may conclude that our preliminary analysis of the TR SRG signal is already an improvement on the initial treatment[9] in that it brings forth the Raman tail as well as the zero-delay feature that are observed in the experiments on liquid CS_2 [see Fig. 2(a)].

2. *Shortcomings of the Gaussian Model: Agreeing and Disagreeing Configurations*

Even after we leave this simple limit situation and incorporate the phase effects and corresponding interferences (mixing term $\mathcal{T}$) discussed above, our theoretical results cannot explain the following striking experimental observations.

First, it is remarkable that for an intentionally set mismatch (τ or τ') in one of the laser pairs and the accordingly expected loss of T_2-signal strength, the latter sharply and strongly recovers when the mismatch is compensated for by the same mismatch in the other laser pair. But even more striking is the observation that the foregoing holds true only when in both pairs either the ω_L pulse or the ω_S pulse is delayed: The signal is almost completely lost if the ω_L pulse

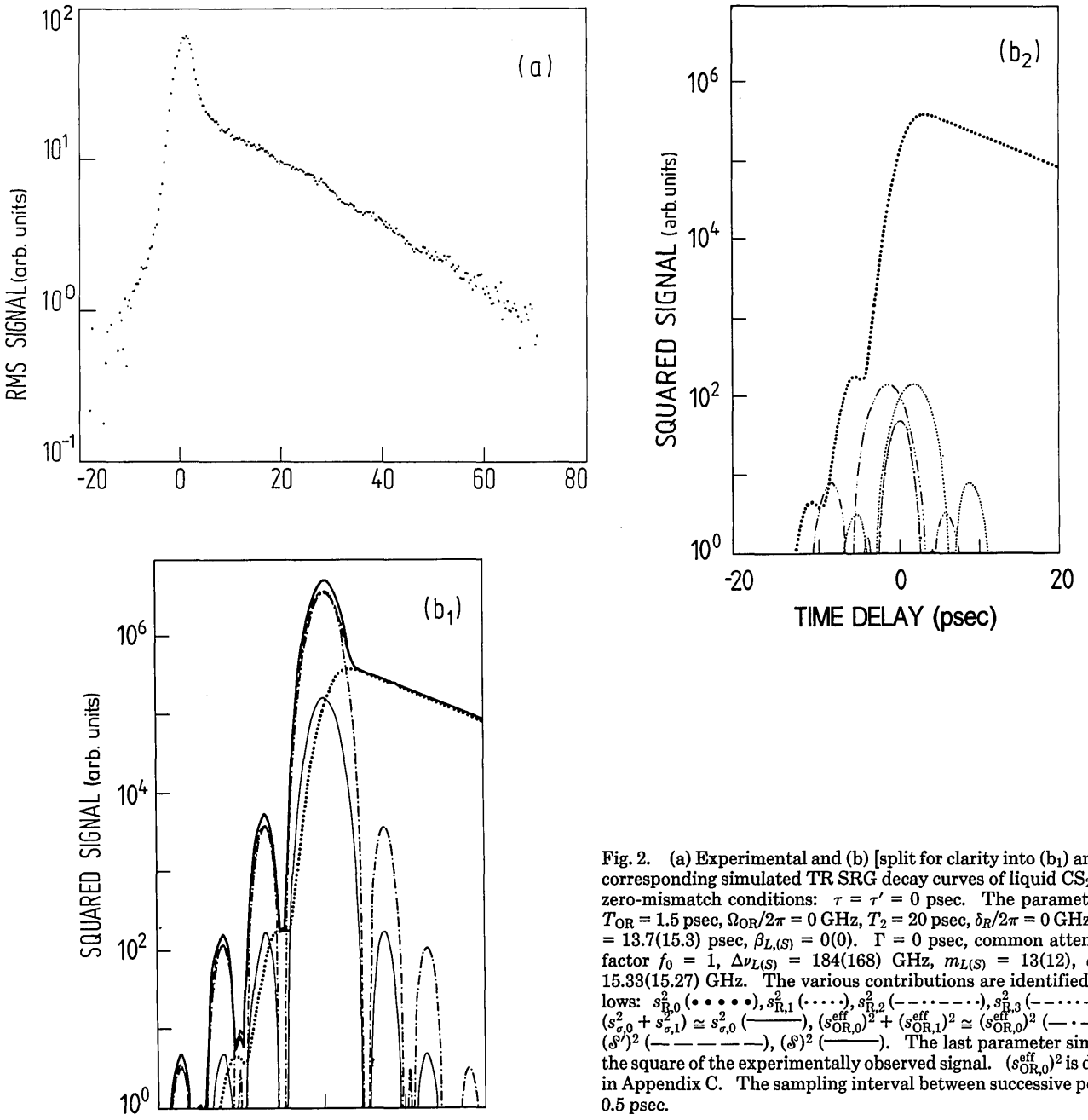

Fig. 2. (a) Experimental and (b) [split for clarity into (b_1) and (b_2)] corresponding simulated TR SRG decay curves of liquid CS_2 under zero-mismatch conditions: $\tau = \tau' = 0$ psec. The parameters are $T_{OR} = 1.5$ psec, $\Omega_{OR}/2\pi = 0$ GHz, $T_2 = 20$ psec, $\delta_R/2\pi = 0$ GHz, $t_{p,L(S)} = 13.7(15.3)$ psec, $\beta_{L,(S)} = 0(0)$. $\Gamma = 0$ psec, common attenuation factor $f_0 = 1$, $\Delta\nu_{L(S)} = 184(168)$ GHz, $m_{L(S)} = 13(12)$, $\delta_{L(S)} = 15.33(15.27)$ GHz. The various contributions are identified as follows: $s^2_{R,0}$ (• • • • •), $s^2_{R,1}$ (·····), $s^2_{R,2}$ (– – · · · · · · –), $s^2_{R,3}$ (– – · · · · · · · · –), $(s^2_{\sigma,0} + s^2_{\sigma,1}) \cong s^2_{\sigma,0}$ (———), $(s^{eff}_{OR,0})^2 + (s^{eff}_{OR,1})^2 \cong (s^{eff}_{OR,0})^2$ (— · — · —), $(\mathcal{S}')^2$ (— — — — —), $(\mathcal{S})^2$ (———). The last parameter simulates the square of the experimentally observed signal. $(s^{eff}_{OR,0})^2$ is defined in Appendix C. The sampling interval between successive points is 0.5 psec.

is delayed in one pair and the ω_S pulse in the other, even when the delays are of equal absolute magnitude.

Our theoretical analysis so far predicts the former observations but, at least for ω_L and ω_S pulses of similar characteristics, not the clear distinction between the former and the latter.

From now on these two pulse sequences will be referred to as the agreeing and disagreeing configurations, respectively.

A second experimental fact that merits attention is the sharpness of the signal peak in CS_2 at zero delay. It turns out to be impossible to find a set of pulse parameters that yields, on the one hand, the zero-delay peak's FWHM and height relative to the Raman tail and, on the other hand, the signal strength recovery as a function of $\tau = \tau'$ in the aforementioned agreeing configuration. Finally, it is observed that a mismatch in only one pair causes not only a time shift of the zero-delay peak, as theory predicts, but also a noticeable splitting of it.

Explicit examples and data are discussed in Subsection 4.D.

3. *Incorporating the Domain Model for Mode-Locked Dye-Laser Pulses*

We strongly believe that it is the dye-laser pulse-coherence properties that dominate the phenomena that we have just described. Indeed, any adequate analysis of the coherent excitation and probing experiments must take into account the coherence characteristics of the stimulating fields (cf. Refs. 5, 10, and 28).

Additionally, in order to improve the agreement between

numerical fits and experimental data, time jitter between both dye lasers and spatial wave-vector mismatch factors are again incorporated into the analysis, as explained above.

The competition between pulse-coherence characteristics on the one hand and pulse-duration characteristics on the other is included through the adoption of the so-called domain model[14] for the dye-laser pulses. We recently presented evidence for the existence of domain-structured pulses.[15]

For reasons of mathematical simplicity, the model is cut down to its essentials. Thus each dye laser's oscillator bandwidth is divided into M equally spaced (by δ) spectral domains of identical characteristics. Each domain is assumed to possess the same pulse characteristics as were previously taken for the whole pulse. Thus for each of the dye lasers the field E is specified as

$$E(t)\exp(-i\omega t) = \exp\left(-\frac{a}{2}t^2\right)\exp\left(i\frac{a}{2}\beta t^2\right) \times \exp(-i\omega t)\frac{1}{M}\sum_{m=-\frac{M-1}{2}}^{m=+\frac{M-1}{2}}\exp(-im\delta t), \quad (13)$$

instead of Eqs. (10). Here $(\omega + m\delta)$ is the center frequency of the mth domain. It is evident that the parameters of the two lasers may have different values. We note that an inverse proportionality relation holds between $\sqrt{a}$ and the pulse-envelope duration t_p and between the spectral width $\Delta\omega = M\delta$ and the pulse-coherence time t_c.

When the domain model [Eq. (13)] is plugged into the integral expressions for the dephasing signal (Appendix A), each contribution becomes a fourfold sum over the domains. However, this sum is found[17] to be reducible to a twofold one, essentially for two reasons: the spectral structures of both dye lasers are uncorrelated, and mutually different domains ($m \neq m'$) within the same laser field cannot be phase matched in the interaction process over many pulse periods.

Analytical expressions for the TR SRG-signal have been developed[17] for an arbitrary but fixed pair ($\delta_L \equiv m_L\delta_L$, $\delta_S \equiv m_S\delta_S$), and the results are given in Appendix C. The summation over the domains is done numerically (Subsection 4.C). In Appendix C the jitter (Γ) is taken up as a fixed value; an overall signal loss already appears.

As for the terms in Φ_i, the constant phases of the spatial-mismatch factors have been suppressed because they are of no importance for the contributions separately and because their dependence on the pulse sequence is analogous to that of the pulse phases. Besides, this last property makes them vanish in the interference term $\mathcal{T}$ just as for the pulse phases (ϕ).

For any value of τ, τ', and t_D, similar arguments justify the neglect in the numerical treatment (Subsection 4.C) of the ω terms in Φ_i.

C. Numerical Treatment of the Final Expression for the TR SRG Signal

As was indicated above, the analytical expressions of Appendix C imply in each contribution that a complex summation must be made over the domain structure of each laser field in order for the actually observed TR SRG signal to be obtained. The numerical treatment required for it has enabled us to study the role of all interplaying parameters and to simulate our experimental results. It takes into account our experimental conditions, among which are the spatial-mismatch factors m_i ($i = 0, 1, 2$) as given in Appendix C. To simulate jitter, the parameter Γ is averaged over a few picoseconds (parameter Γ_{abs}) through numerical Gauss integration between $+\Gamma_{abs}$ and $-\Gamma_{abs}$. Moreover, we checked that the relative scaling among the different sample intrinsic contributions for liquid CS_2 given in Eqs. (9) is appropriate for simulating the corresponding experiments.

One requires above all that the qualitative features of the experiments be reproduced by the simulations. Indeed, the susceptibility of the measurements to uncontrollable external parameters makes quantitative data not so reproducible, and the applied domain model is probably too rigid to reproduce all the details of the experiments.[15] Nevertheless, our quantitative results are surely reliable to within an order of magnitude or better.

The dye-laser pulse-parameter values employed in all the simulated dephasing curves that we have presented—except those in Figs. 4 and 7 below—are given in the caption of Fig. 2. They have been adapted from independent experimental observations[15] and adjusted for the best agreement between experimental data and numerical results. Exact matching of the spectral parameters of both dye lasers has been avoided for consistency with the physical assumptions made in the theoretical analysis (Subsection 4.B.3). They are listed in frequency instead of angular-frequency units. It was found that any realistic deviation from symmetrical line shape and/or the presence of linear frequency chirping induces no clearly observable systematic effects in the computed total signal.

For clarity all signal contributions (squared) are drawn separately, together with their sum both with ($\mathcal{S}^2$) and without ($\mathcal{S}'^2$) addition of the interference term $\mathcal{T}$. The limit of completely collinear signal generation has been taken.[17] Furthermore, the dynamic range of the simulations has been extended over more than 2 orders of magnitude, which is the maximum reached in the experiments on CS_2.

The common key to the plots is given in the caption of Fig. 2. All plots are scaled vertically to the same arbitrary units. Beforehand, however, the common attenuation factor f_0 [Eq. (11)] is split off: It is listed with the plot parameters.

We now comment on our principal conclusions, in the light of some typical results (Figs. 2–4).

D. Discussion of Dephasing Signal Characteristics: Experimental Observations versus Numerical Simulations

1. *Zero-Delay-Peak Width*

Inspection of the integral expressions (Appendix A) for the dephasing signal with $\tau = \tau' = 0$ discloses their similarity to those for a (first-order) field-visibility curve rather than those for a (second-order) intensity autocorrelation or cross-correlation curve, even for the Raman terms.[29] This is a first confirmation of the phase sensitivity and phase memory in the TR SRG experiments.

In the case of CS_2 and our experimental configuration, the observed signal peak near zero delay (cf. Fig. 2) is made up mainly of the $s_{\sigma,0}$ and $s_{OR,0}$ contributions. Thus its FWHM

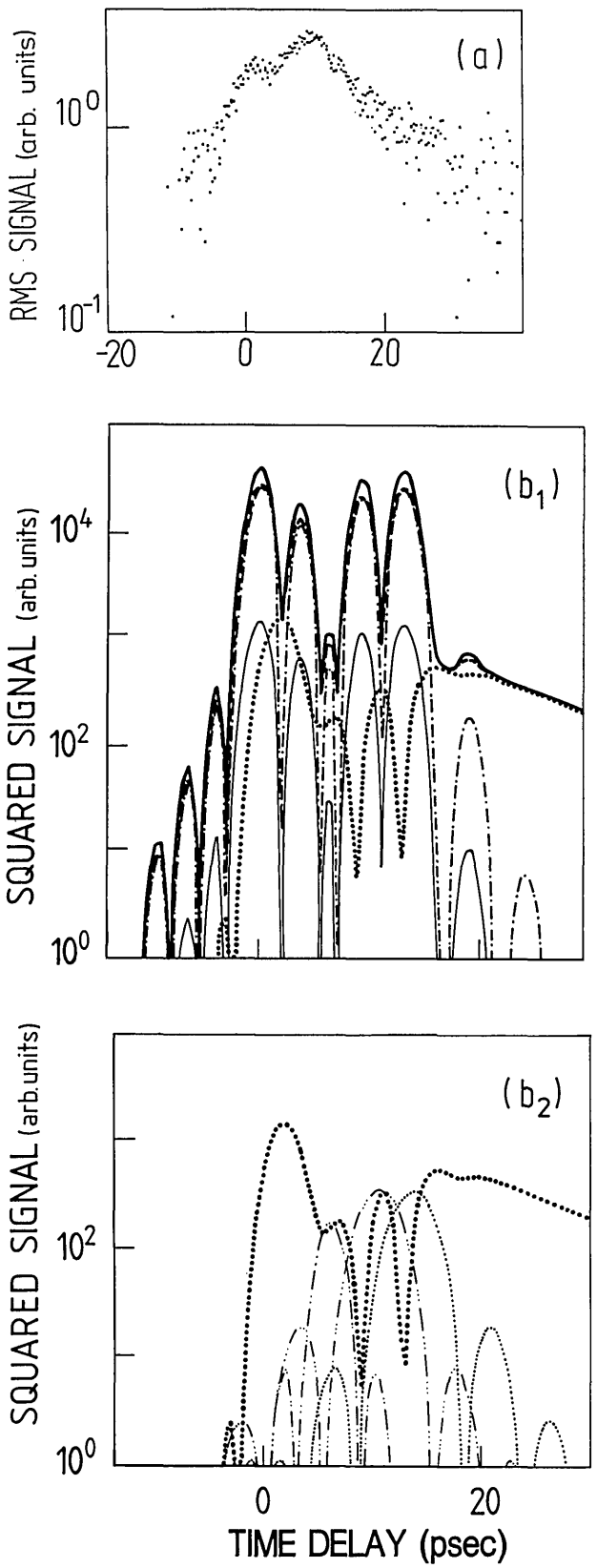

Fig. 3. (a) Experimental and (b_1), (b_2) corresponding simulated decay curves of liquid CS_2 under the mismatch conditions $\tau \neq 0$, $\tau' = 0$. (a): $\tau = 10$ psec, $\tau' = 0$ psec. For the key to (b_1) and (b_2) see Fig. 2, whose parameters for (b_1) and (b_2) are the same except that here $\tau = 12$ psec, $\tau' = 0$ psec, and common attenuation factor $f_0 = 0.62$.

is approximated well by that of the product of the visibility curves of both dye lasers, by which

$$\mathrm{FWHM} = \frac{\mathrm{FWHM}^{\mathrm{envelope}} \times \mathrm{FWHM}^{\mathrm{coh}}}{[(\mathrm{FWHM}^{\mathrm{envelope}})^2 + (\mathrm{FWHM}^{\mathrm{coh}})^2]^{1/2}}. \quad (14)$$

Here, $\mathrm{FWHM}^{\mathrm{envelope}}$ represents the correlation width due solely to the pulse envelopes:

$$\mathrm{FWHM}^{\mathrm{envelope}} \simeq 4\left[\frac{\ln 2(a_L + a_S)}{(a_L + a_S)^2 + (a_L\beta_L - a_S\beta_S)^2}\right]^{1/2}, \quad (15)$$

and $\mathrm{FWHM}^{\mathrm{coh}}$ the one due solely to the domain structure:

$$\mathrm{FWHM}^{\mathrm{coh}} \simeq \frac{2\sqrt{3}}{\pi} \times \left\{\left(\frac{2\pi}{M_L\delta_L}\right)^2 + \left(\frac{2\pi}{M_S\delta_S}\right)^2 - \left[\left(\frac{2\pi}{M_L\delta_L}\right)^4 + \left(\frac{2\pi}{M_S\delta_S}\right)^4\right]^{1/2}\right\}^{1/2}. \quad (16)$$

Note that $(2\sqrt{3}/\pi)$ $[2\pi/M_{L,(S)}\delta_{L,(S)}]$ equals the $\mathrm{FWHM}^{\mathrm{coh}}_{L,(S)}$ of each laser separately.

It is clear that the smallest among the last two, i.e., $\mathrm{FWHM}^{\mathrm{coh}}$, is the one that restricts the observed FWHM.

Frequency chirping comes in systematically through the squared difference between the spectral broadening parameters of both dye lasers, i.e., $(a_L\beta_L - a_S\beta_S)^2$. In a different geometrical configuration, however, the $s_{\sigma,1}$ and $s_{\mathrm{OR},1}$ contributions might gain in relative importance; according to the integral expressions in Appendix A their effect on $\mathrm{FWHM}^{\mathrm{envelope}}$ [relations (15)] follows an $(a_L\beta_L + a_S\beta_S)^2$ instead of an $(a_L\beta_L - a_S\beta_S)^2$ dependence.

The convolution that appears in the orientational contributions (memory time T_{OR}) affects practically only the strength of the peak, not its shape or width. Moreover, under detuning from the Raman vibrational resonance ($\delta_R \neq 0$), the signal peak becomes less subject to these vibrational contributions (Subsection 4.D.4). As a result, the pulse parameters can be carefully checked.

2. *Coherence Effects*

Many signal features, among which is the occurrence of a signal peak at zero delay, are dominated by the aforementioned coherent coupling effects (Subsection 4.A), a concept that is adapted from picosecond pump and probe absorption experiments.[29–33] However, in our extended meaning (cf. Ref. 10) the concept points to interferences in which time-delayed replicas of more than one laser field are involved, together with different specific timing sequences. Therefore the coherence artifact has quite a different appearance, and it is discovered (Appendix A) in the s_σ and s_{OR} contributions

$$\text{at } t_D = 0 \qquad \text{for the } \omega_S \text{ pulses}$$

and

$$\text{at } t_D = \tau - \tau' \qquad \text{for the } \omega_L \text{ pulses.} \quad (17)$$

The closer to each other these two situations occur, the stronger the coherence effects, because of the superimposed overlap effect of the pulse envelopes.

As has been suggested by Oudar,[10] the coherence effects also influence the resonant vibrational contributions. This

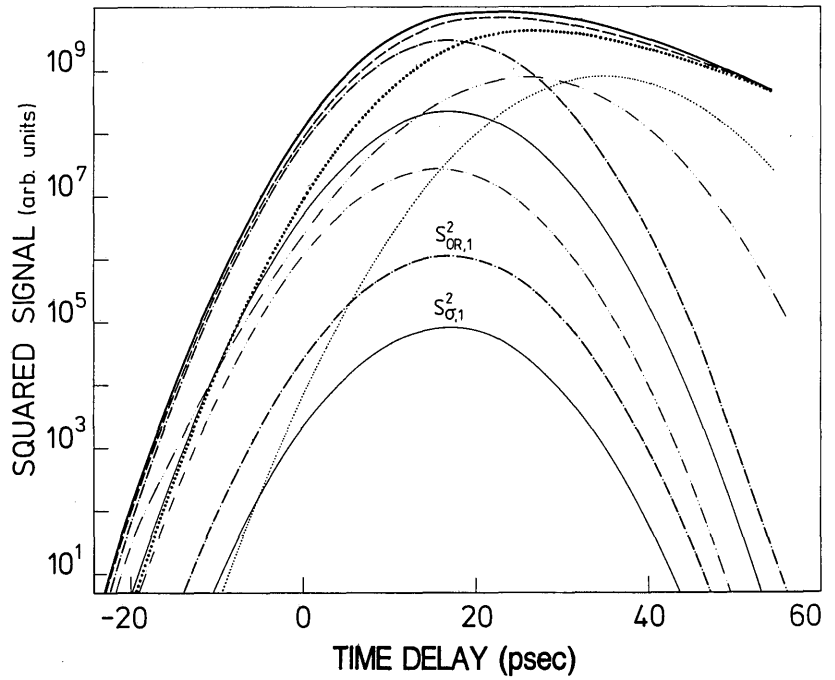

Fig. 4. Illustration of coherent coupling effects in simulated decay curves of liquid CS_2 under mismatch conditions ($\tau \neq 0$, $\tau' = 0$) but neglecting the laser-pulse domain structure. The separate orientational, $s^2_{OR,1}$, and instantaneous, $s^2_{\sigma,1}$, contributions are drawn in order to display their different behavior with regard to width (Subsection 4.D.1). The parameters are the same as for Fig. 2 except that $\Delta\nu_{L(S)} = 0(0)$ GHz, $\tau = 30$ psec, $f_0 = 0.52$.

happens provided that the timing sequence within the exciting (ω_L, ω_S) pair is the same as that within the probing pair, i.e., when

$$\begin{aligned} \text{for } s_{R,0}: &\quad \tau = \tau', \text{ irrespective of } t_D, \\ \text{for } s_{R,2}: &\quad t_D = \tfrac{1}{2}(\tau - \tau'), \\ \text{for } s_{R,1} \text{ and } s_{R,3}: &\quad t_D = \tau - \tau'. \end{aligned} \tag{18}$$

It is understood that the phase pattern generated during excitation is memorized by the material and (partially) recovered in the probing process. Therefore the occurrence of this coherence effect is slightly delayed and smoothed as a result of the material's response time T_2, in contrast to the immediacy of the interferences in the s_σ and s_{OR} terms. For the latter, the orientational relaxation time T_{OR} occurs through the overlap of the pulse envelopes only.

In the analytical expressions for the dephasing signal $\mathcal{S}(t_D)$ (Appendix C) the circumstances indicated [Eqs. (17) and (18)] coincide with a minimal coupling between the parameters t_D, τ, and/or τ', on the one hand, and, on the other hand, the parameters related to the imperfect coherence of the laser pulses. The latter parameters are $\delta_L - \delta_S$ for the Raman terms, δ_L and δ_S separately (at $t_D = \tau - \tau'$ and $t_D = 0$, respectively) for the electronic (s_σ) and orientational (s_{OR}) contributions, and β_L and β_S. The coherence effect acts instantaneously if δ_L and δ_S do not appear in the error function's argument, and vice versa [cf. relations (12)].

In conclusion, the coherent coupling effect means that the superposition of mutually unrelated interferences that under general circumstances blurs the coherent signal generation gets completely constructive under the specific interaction conditions of Eqs. (17) and (18). Stated otherwise, the deficiency in coherence of the laser fields has no, or minimal, influence on the TR SRG signal, and a peak develops in the latter. For the vibrational Raman contributions, the peaks are less pronounced and slightly shifted.

3. *Signal Behavior for Temporally Mismatched Pulse Pairs*

The foregoing considerations permit a full understanding of the TR SRG signal's behavior under conditions of temporally mismatched pulse pairs ($\tau, \tau' \neq 0$).

a. *Arbitrary Timing Mismatches in Pump and Probe Pair*

Suppose that the dye lasers are tuned for probing the Raman-active vibration in liquid CS_2 (656 cm^{-1}) and that a sequence of delay (t_D) scans is performed for increasing values of mismatch τ within the pump pair ($\tau' = 0$). The experiments and corresponding numerical simulations agree for the following observations.[17] Starting from $\tau = 0$ (cf. Fig. 2), three regions in τ-parameter space may be distinguished as τ is varied from less than ~4 psec to more than ~7 psec (Fig. 3). First the peak shifts over approximately half of the mismatch value, with conservation of the main T_2 decay features. While shifting further, the peak gradually broadens, and the T_2 decay becomes imperceptible. Finally (Fig. 3), the peak splits into two components of approximately equal strength, the slightly weaker one at zero-delay time and the other at a delay point equal to τ. The latter trend develops further, and the peak at $t_D = 0$ may disappear. The overall signal strength diminishes quickly.

Introducing a similar mismatch into the pump pair and none into the probe pair [i.e., $(\tau, 0)$ by $(0, \tau' \equiv \tau)$; cf. Subsec-

tion 4.A], or changing τ to $-\tau$, approximately generates the mirror images near $t_D = 0$ of these plots as far as the occurrence of peaks is concerned. The T_2 decay is equally lost from the midregion on. This was partially predicted above.

The above characteristics originate from the competition between the effects due to the coherent-coupling [cf. Eqs. (17) and (18)] and the ones due to the overlap of the pulse envelopes.

The time positions of the signal maxima as they would occur if merely the pulse-envelope overlap were acting can be derived from the expressions in Appendix B.[17] With respect to the four vibrational Raman contributions ($s_{R,0}$ to $s_{R,3}$), these positions are influenced by the relaxation time T_2 through the latter's coupling with t_D in the error functions.

The coherent coupling effects influence the location of total signal enhancements, predominantly through their effect on the s_σ and s_{OR} contributions. The behavior of these contributions under time-mismatch conditions (Appendix A) resembles that of the product of the visibility curves of both dye lasers, shifted with respect to each other over $\Delta = \tau - \tau'$, the relative mismatch difference. The peaking of the corresponding curves at $t_D = 0$ displays mainly the coherence properties of the ω_S field, and the peaking at $t_D = \Delta$ ($t_D = \tau$ for $\tau' = 0$) those of the ω_L field. Nevertheless, depending on specific (τ, τ') values, some combined influence of both visibility curves may always show up. Also, in the $s_{R,0}$ to $s_{R,3}$ terms one recognizes coherence effects that analogously originate in the ω_L and ω_S fields separately: they are of minor relevance.[17] On the other hand, the ones that originate in the effective ($\omega_L - \omega_S$) field [cf. Eqs. (18)] dominate the phenomena discussed below in Subsection 4.D.3.b.

We have investigated numerically[17] how the coherence properties of both fields relative to each other play a part in the signal characteristics.

The coherence peak near zero delay becomes less pronounced with an increasing coherence time of the relevant laser field; it disappears in the limit of full coherence. If, in particular, both fields are fully coherent, i.e., if pure Gaussian envelopes are adopted (Fig. 4), the overall signal has much higher gain, but its behavior is reduced to that of the relatively broad pulse envelopes. The undeniable experimental characteristics anticipated in Subsection 4.B.2 cannot be reproduced.

Furthermore, the deficiencies are not relieved if frequency chirping is included, although now the latter's effect is clearly visible. In general it is indeed observed[17] that the influence of a chirp is greater if it is chirp only that limits the laser field coherence time, i.e., when the domain structure of the pulses is left out of the simulations.

We conclude that the boundaries of the three experimentally distinguished regions, starting from $\tau = 0$, are set by, respectively, the combined coherence time, i.e., the FWHM of the product visibility curve ($\simeq$4.3 psec in our numerical simulation) and the largest of the widths of the separate visibility curves (ω_L laser, $\simeq$5.5 psec; ω_S laser, $\simeq$6.0 psec).

Moreover, the performance of TR SRG experiments with mismatched laser pairs is useful for two reasons.[17] Compared with the natural $\tau = \tau' = 0$ condition, it permits a more accurate evaluation of the separate pulse characteristics of both stimulating laser fields (cf. Figs. 2–4 and related discussions) and a better discrimination of certain sample intrinsic contributions, because it alters their relative weights. To the same end, a modified spatial configuration may be helpful.[17]

b. Mutually Equal Mismatches in Pump and Probe Pair

The evidence strongly points to the fact that the coherent coupling effects are responsible for the strong discrepancy between agreeing and disagreeing configurations (Subsection 4.B.2).

For agreeing configurations the principal signal features are conserved, among which are the appearance of a unique zero-delay peak, the decay behavior and time, and the strength ratio of peak to tail. The signal loss is quasi-uniform over the whole curve. It goes by the intensity cross correlation of the pulse envelopes, i.e., for Gaussian envelopes, by $\exp[(a_L a_S \tau^2)/(a_L + a_S)]$.

A completely different behavior is observed experimentally in the disagreeing configurations, i.e., under the imposition of an identical delay (or advance) τ on pulses of different color within each laser pair. Already at values of τ smaller than the combined coherence time any T_2 evaluation becomes impossible because the peak is broadened and its strength reduced to $\sim$15%. Before the complete loss of any observable signal, the weak residual peak seems to split into two or three shifted, badly defined ones.

With respect to the corresponding numerical simulations, it must be stressed that only after the domain structure was taken into account could this clear discrepancy between both cases be reproduced[17]; otherwise the disagreeing configuration yielded an even stronger recovery than the agreeing one.

In particular, the unique recovery of the Raman tail for $\tau = \tau'$ has been assigned to coherent coupling of the effective ($\omega_L - \omega_S$) field in the main Raman term $s_{R,0}$. This follows from an examination of this main Raman term separately as a function of the relative mismatch $\Delta = \tau - \tau'$ and the parameters τ' and t_D.[17] We show three-dimensional views of them in Fig. 5. As long as the domain structure is not incorporated, the maximum signal is found close to the diagonal [Fig. 5(a)]. Its exact location is dependent on the pulse-envelope parameters a_L and a_S relative to T_2 and, only within a certain range, on t_D. But this diagonal behavior does not agree with experiment. However, after the domain structure is taken into account, a pattern closely resembling the product of the visibility curves of this coherence structure is superimposed upon it, as shown, e.g., in Fig. 5(b). The $\Delta = 0$ cross line is indeed strongly favored. The maxima in the mismatch difference Δ coincide with constructive interferences of the arguments involved in the sum over the domains. The fact that they are not lying symmetrically around the strongest maximum ($\Delta = 0$) is due to the existence of spectral mismatches between the interacting domains of both dye lasers.

Therefore our most important conclusions are that an experimental check of the singularity of the agreeing configuration points to the existence of domain structure in the stimulating laser fields and that the signal loss as function of τ discloses the mean pulse-envelope width.

4. Spectral Analysis of the TR SRG Signal

Studying the TR SRG signal characteristics under detuning from the vibrational Raman-resonance condition offers a better distinction between the sample intrinsic on the one

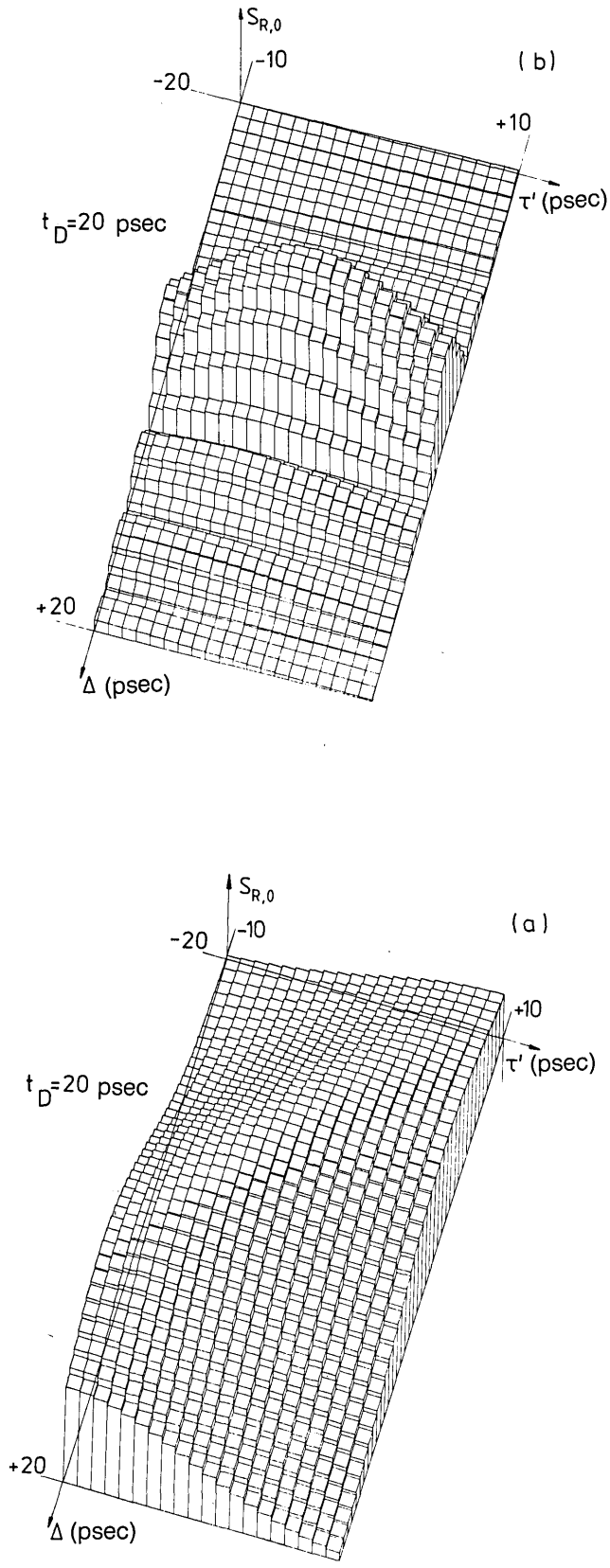

Fig. 5. Illustration of the uniqueness of the agreeing configuration ($\tau = \tau'$): Recovery of the signal modulus as a function of the relative mismatch $\Delta = \tau - \tau'$ and τ' (−10 psec → +10 psec). The parameters for (a) are the same as in Fig. 2 except that $\Delta\nu_{L(S)} = 0(0)$ GHz. The parameters for (b) are the same as for (a) except that $\Delta\nu_{L(S)}$ are the same as for Fig. 2(b).

hand, and, on the other hand, the pulse properties. Two types of examination have been performed: either a delay scan at fixed value of the detuning δ_R or a δ_R scan at a fixed delay position t_D.

The larger the relaxation time T_2, i.e., the smaller the resonance linewidth, the larger the signal's susceptibility to $|\delta_R|$. The detuning is relevant only for the Raman contributions and influences the interference term $\mathcal{T}$ through them. As a result, raising the absolute value of the detuning $|\delta_R|$ makes the orientational and electronic terms near zero delay gradually dominate the observed signal. The time lag of the main Raman term shrinks to zero, and it acquires the same shape as the previous terms. Finally, when $|\delta_R|$ is large compared with $1/t_c$, any vibrational excitation is excluded: The signal is centered at and symmetrical near the zero-delay time and reflects purely pulse-coherence and envelope properties (see Ref. 15).

With respect to the signal behavior versus δ_R, a sequence of experiments and corresponding simulations is included in Figs. 6 and 7 (the parameter is t_D). Zero detuning is determined experimentally as being the δ_R value for which maximum signal strength occurs, at an arbitrary delay point in the Raman tail well beyond the peak.

The examples prove that the observed spectrum (i.e., the structure near zero detuning and the subsequent decrease) results from adding to the main Raman contribution the orientational and electronic ones, together with their mutual interference terms. The asymmetry between plus and minus δ_R values, also observed in the first type of investigation, i.e., delay scans with δ_R fixed, arises mainly through the change of $\mathcal{T}$ connected with the change in sign of the argument of the main Raman term. The dependence on t_D reflects the different time responses of the various contributions.

Therefore we have proved that the same sample intrinsic information can be probed, e.g., in steady-state CARS spectroscopy, which may be interpreted in terms of the sum and interferences of imaginary and real parts of the medium's $\chi^{(3)}$ tensor.[34] Comparable observations of the aforementioned time dependence have been reported in related spectroscopic techniques,[35–37] among which is pulse-sequenced CARS.[36]

In addition, we have demonstrated that the observed curve displays an entanglement of the pure CARS line shape with the pulse's spectral structure. Such experimental artifacts have received little attention in the past. Therefore we have compared our results for domain-structured pulses (Figs. 6 and 7) with the usual CARS line shape as it is obtained with pure Gaussian (transform-limited) pulses.[17] We note (i) the flat spectral structure for delays smaller than the combined coherence time, nevertheless exhibiting the characteristic dip on the negative δ_R side [Figs. 6(a) and 7(a)], (ii) the occurrence of extra peaks and dips aside from the main Raman peak [Figs. 6(b) and 7(b)], and (iii) the final tendency to the pure but broadened and correspondingly weakened Raman term only [Figs. 6(c) and 7(c)]. The broadening corresponds to the spectral resolution, which is set by the bandwidths of the laser fields. Note that the FWHM of the total observed signal is still dependent on t_D. So is the shift of the observed maximum toward positive δ_R values, which shrinks to zero as t_D rises. This shift would not exist if the interferences $\mathcal{T}$ were not accounted for. The

dependence on t_D of the main Raman term itself is much weaker.

According to the specific pulse parameters chosen, some features show up more or less pronounced, eventually shifted on the δ_R axis. This is the reason why in Fig. 7(b) a different set of pulse parameters has been used for illustration. The spatial geometry is of minimal influence since mainly terms of equal spatial mismatch factors are interfering.

In conclusion, the deviation from perfect coherence represented by the domain model seriously affects the observed spectral behavior of the TR SRG signal. This must be taken into account in any spectral analysis, together with the relative portion of all sample contributions, as they appear in $|\chi^{(3)}|$.

5. Time-Resolution and Intrinsic Material Parameters

It has been proved that T_2 governs the decay of the main Raman term in a t_D scan, with a time resolution ultimately set by the combined coherence time of both stimulating fields and not by the cross-correlation width of the pulse envelopes. Our similar study of C_6H_6 ($T_2 \approx 4.4$ psec) has confirmed this.[17] Contrary to the statement made in Ref. 9, we find that the relaxation time T_{OR} of the orientational motion cannot be determined fundamentally from a t_D scan because T_{OR} is not essentially connected to the delay time t_D of the probing process. The property that a different value of T_{OR} changes the relative portion of the orientational contributions is impractical for a T_{OR} determination because of the uncertainty about all other parameters. The coupling between T_{OR} and (τ, τ') is stronger, but until now no systematic effects could be discovered that are suitable for the determination of this relaxation time.

If Ω_{OR} is different from zero, the main result is a weakening of the orientational contributions.

The susceptibility to time jitter Γ between the pulse envelopes increases the closer the experimental geometry approaches the completely collinear one. At $\leqq 3$ psec of absolute value, however, its influence is almost negligible.

The experiment often showed a weak oscillation of ~13 psec in the T_2 tail for exact Raman resonance ($\delta_R = 0$) with the strongest mode, which cannot be simulated in any acceptable way within the present theory. Exact incorporation of the dye-laser mode structure within one domain,[25,28,38,39] instead of the assumption of a Gaussian envelope profile, will not explain this. One would get oscillations on both sides of the zero-delay peak,[15] in contradiction to the observed asymmetry.

However, these oscillations are readily explained by taking into account the weaker Raman modes due to combination bands and isotope effects. In spontaneous Raman scattering on CS_2 we confirmed the presence of four weaker Raman modes, all on the low-frequency side of the strongest mode (656 cm^{-1}) and with frequency differences $\Delta\nu$ of, respectively, 9.6, 8.0, 5.0, and 2.6 cm^{-1}. These modes were not taken into account in our simulations. Simultaneous excitation of these Raman modes owing to the broad dye-laser bandwidth leads to beating[5,6,39,40] in the T_2 decay with a period T equal to the difference in the Raman frequencies: $T = 1/\Delta\nu$. The observed beating periods of 13 and 3.5 psec can, within experimental error, be related to the Raman modes with frequency differences of 2.6 and 9.6 cm^{-1}, respectively. In order to observe the 3.5-psec beating we had to select a positive detuning ($\delta_R > 0$) so as to excite the weak Raman mode strongly enough. The other low-frequency Raman modes gave no observable beating, as either they were too weak or their line widths were too broad, corresponding to a faster decay. For negative detunings we found no beatings in accordance with the spontaneous Raman spectrum. Pronounced beatings of similar origin have been observed in solid para H_2.[41]

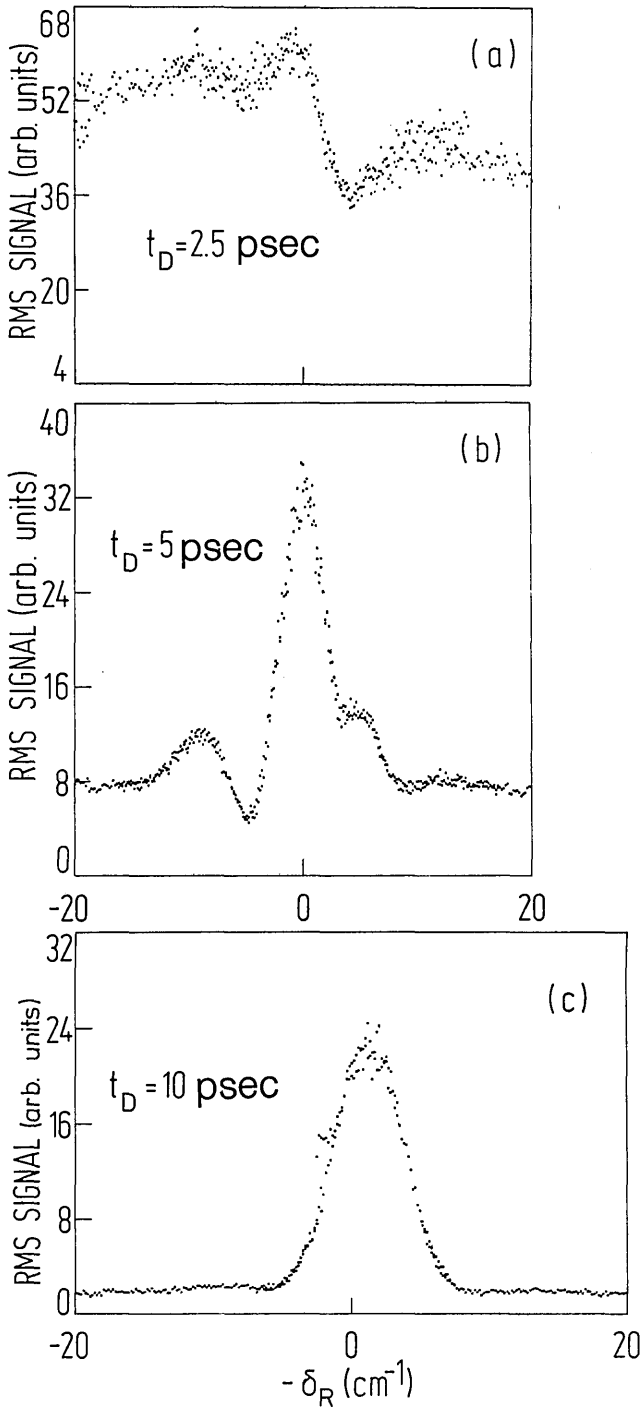

Fig. 6. Experimental wave-number scans at a fixed delay (t_D) between pump and probe pair on a liquid CS_2 sample: (a) t_D = 2.5 psec, (b) t_D= 5 psec, (c) t_D = 10 psec.

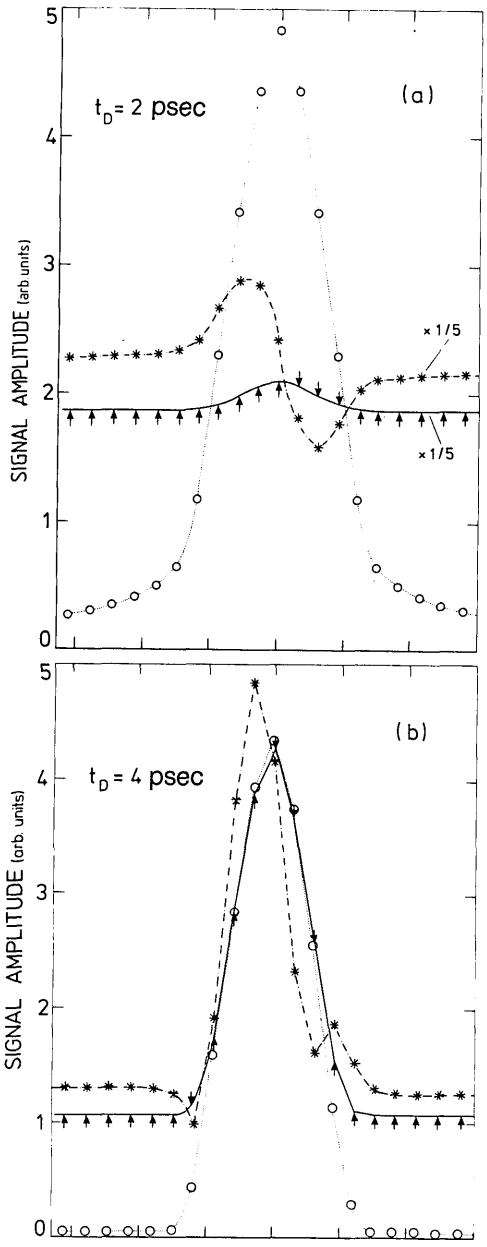

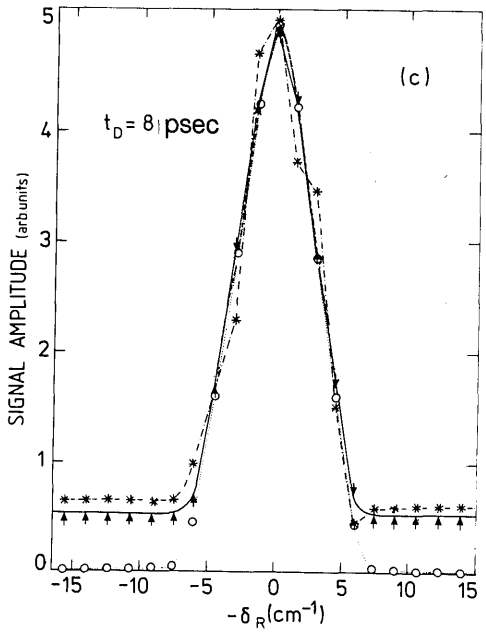

Fig. 7. Numerical simulations corresponding to Fig. 6: o, modulus of the pure Raman ($|s_{R,0}|$) contribution; ↑, sum signal $\mathcal{S}'$ disregarding interference; *, sum signal $\mathcal{S}$ including interferences, simulating the observed signal. (a) $t_D = 2$ psec, (b) $t_D = 4$ psec, (c) $t_D = 8$ psec. Equal scaling applies to (a)–(c). In (a) and (c) the usual pulse and material parameters have been adopted [see Fig. 2(b)]. Slightly different pulse parameters were chosen for (b): they accentuate the features but do not alter them essentially. They are $t_{p,L} = 8.0$ psec, $\beta_L = 0$, $\Delta\nu_L = 170$ GHz, $m_L = 11$, $\delta_L = 17$ GHz, $t_{p,S} = 9.8$ psec, $\beta_S = 0$, $\Delta\nu_S = 158$ GHz, $m_S = 12$, $\delta_S = 14.36$ GHz, spectral skewness $L(S) = 1.13(1)$.

5. CONCLUSION

The theoretical analysis of the time-resolved stimulated-Raman-gain experiment, developed in close agreement with our experimental configuration,[15,16] has explained the interplay of the experimental parameters and the sample characteristics. This analysis improves the understanding of TR SRG spectroscopy and the interpretation of dephasing experiments.

We have proved that both real and imaginary parts of the nonlinear susceptibility tensor contribute to the TR SRG signal,[10,11] to a different extent. Hence, in contrast to its two-beam variant,[17,42] four-beam TR SRG spectroscopy is competitive with steady-state CARS[34] and related techniques with respect to its spectral information content.

Moreover, we have demonstrated how a variation of the experimental conditions permits one to discriminate among the various intrinsic properties of the sample and the external parameters. To this end, the four-beam facility offers additional opportunities.

In particular, the important role of the coherence properties of the laser pulses has been demonstrated. For instance, the signal loss related to the lack of interpulse coherence and the consequent less effective buildup of the signal over many pulse periods has been indicated. So-called coherent coupling effects should not be neglected. In particular, it is the pulse-coherence time that determines the time resolution of the dephasing measurements.

Also, on account of the high sensitivity of the TR SRG experiments, the determination of unknown sample characteristics obviously requires evaluation of the experimental parameters. In what detail and how accurately these parameters need to be known is dependent also on the relationship between sample and pulse parameters. Experiments

that evidence certain of these pulse parameters have been discussed. Nevertheless, we recommend a regular check of a reference measurement to avoid false interpretations. Liquid CS_2 (300 K), for instance, is by now a sufficiently well-characterized candidate.

This study could be extended experimentally as well as theoretically, in particular to different polarization combinations of the exciting and probing fields and different geometrical and/or modulation configurations. For example, the double modulation may be spread over separate beams or could consist of phase and intensity modulation. Moreover, a study of solidified CS_2 could prove useful for distinguishing the orientational parameters clearly.

APPENDIX A: INTEGRAL EXPRESSION FOR THE DEPHASING SIGNAL

The following expression was obtained by substituting into Eq. (2) the timing sequences of the exciting and probing laser pulses (Subsection 3.A) and a model for the time-dependent response of the medium (Subsection 3.B). The subscripts σ, R, and OR identify the electronic, vibrational Raman, and orientational Raman contributions, respectively:

$$\begin{aligned}
\mathcal{S}(t_D) \propto \sigma\,\mathrm{Im}\Big(&\exp\{i[(\phi_{L'}-\phi_{S'})-(\phi_L-\phi_S)]\}M[(k_{L'}-k_{S'})\\
&-(k_L-k_S)]\exp[i(\omega_L-\omega_S)t_D]\exp[-i\omega_L(\tau-\tau')]\\
&\times\int_{-\infty}^{+\infty}dt E_{L'}(t-t_D-\tau'-\Gamma)E_{S'}^*(t-t_D)\\
&\times E_L^*(t-\tau-\Gamma)E_S(t) \qquad (s_{\sigma,0})\\
&+\exp\{i[-(\phi_{L'}+\phi_{S'})+(\phi_L+\phi_S)]\}M[-(k_{L'}+k_{S'})\\
&+(k_L+k_S)]\exp[-i(\omega_L+\omega_S)t_D]exp[i\omega_L(\tau-\tau')]\\
&\times\int_{-\infty}^{+\infty}dt E_{L'}^*(t-t_D-\tau'-\Gamma)E_{S'}^*(t-t_D)\\
&\times E_L(t-\tau-\Gamma)E_S(t)\Big) \qquad (s_{\sigma,1})\\
+\,\mathrm{Im}\Big(&\exp\{i[(\phi_{L'}-\phi_{S'})-(\phi_L-\phi_S)]\}\\
&\times M[(k_{L'}-k_{S'})-(k_L-k_S)]\\
&\times\exp[i(\omega_L-\omega_S)t_D]\exp[-i\omega_L(\tau-\tau')]\\
&\times\int_{-\infty}^{+\infty}dt\Big[E_S(t)E_{S'}^*(t-t_D)\\
&\times\int_{-\infty}^{t}dz d_{\mathrm{OR}}(t-z)E_{L'}(z-t_D-\tau'-\Gamma)\\
&\times E_L^*(z-\tau-\Gamma)\Big] \qquad (s_{\mathrm{OR},0})\\
&+\exp\{i[-(\phi_{L'}+\phi_{S'})+(\phi_L+\phi_S)]\}M[-(k_{L'}+k_{S'})\\
&+(k_L+k_S)]\exp[-i(\omega_L+\omega_S)t_D]\exp[i\omega_L(\tau-\tau')]\\
&\times\int_{-\infty}^{+\infty}dt\Big[E_S(t)E_{S'}^*(t-t_D)\int_{-\infty}^{t}dz d_{\mathrm{OR}}(t-z)\\
&\times E_{L'}^*(z-t_D-\tau'-\Gamma)E_L(z-\tau-\Gamma)\Big] \qquad (s_{\mathrm{OR},1})\\
&+\exp\{i[(\phi_{L'}-\phi_{S'})-(\phi_L-\phi_S)]\}M[(k_{L'}-k_{S'})\\
&-(k_L-k_S)]\exp[i(\omega_L-\omega_S)t_D]\exp[-i\omega_L(\tau-\tau')]\\
&\times\int_{-\infty}^{+\infty}dt\Big\{\exp[-i(\omega_L-\omega_S)t]E_{L'}(t-t_D-\tau'-\Gamma)\\
&\times E_{S'}^*(t-t_D)\int_{-\infty}^{t}dz d_{\mathrm{R}}(t-z)\exp[i(\omega_L-\omega_S)z]\\
&\times E_L^*(z-\tau-\Gamma)E_S(z)\Big\} \qquad (s_{\mathrm{R},0})\\
&+\exp[i(\phi_{L'}-\phi_L)]M(k_{L'}-k_L)\exp(i\omega_L t_D)\\
&\times\exp[-i\omega_L(\tau-\tau')]\int_{-\infty}^{+\infty}dt\Big\{\exp[-i(\omega_L-\omega_S)t]\\
&\times E_{L'}(t-t_D-\tau'-\Gamma)E_{S'}^*(t-t_D)\int_{-\infty}^{t}dz d_R(t-z)\\
&\times\exp[i(\omega_L-\omega_S)z]E_L^*(z-\tau-\Gamma)E_{S'}(z-t_D)\Big\}\\
&\qquad (s_{\mathrm{R},1})\\
&+\exp\{i[-(\phi_{L'}+\phi_{S'})+(\phi_L+\phi_S)]\}M[-(k_{L'}+k_{S'})\\
&+(k_L+k_S)]\exp[-i(\omega_L+\omega_S)t_D]\exp[i\omega_L(\tau-\tau')]\\
&\times\int_{-\infty}^{+\infty}dt\Big\{\exp[-i(\omega_L-\omega_S)t]E_L(t-\tau-\Gamma)\\
&\times E_{S'}^*(t-t_D)\int_{-\infty}^{t}dz d_R(t-z)\exp[i(\omega_L-\omega_S)z]\\
&\times E_{L'}^*(z-t_D-\tau'-\Gamma)E_S(z)\Big\} \qquad (s_{\mathrm{R},2})\\
&+\exp[-i(\phi_{L'}-\phi_L)]M[-(k_{L'}-k_L)]\exp(-i\omega_L t_D)\\
&\times\exp[i\omega_L(\tau-\tau')]\int_{-\infty}^{+\infty}dt\Big\{\exp[-i(\omega_L-\omega_S)t]\\
&\times E_L(t-\tau-\Gamma)E_{S'}^*(t-t_D)\int_{-\infty}^{t}dz d_R(t-z)\\
&\times\exp[i(\omega_L-\omega_S)z]E_{L'}^*(z-t_D-\tau'-\Gamma)\\
&\times E_{S'}(z-t_D)\Big\}\Big). \qquad (s_{\mathrm{R},3})
\end{aligned}$$

APPENDIX B: ANALYTICAL EXPRESSIONS FOR THE DEPHASING SIGNAL

The various TR SRG contributions for the cases of zero frequency chirp ($\beta_L = \beta_S = 0$), zero jitter ($\Gamma = 0$), zero resonance detuning ($\delta_R = 0$), and zero orientational frequen-

cy ($\Omega_{OR} = 0$) are given below. Spatial-mismatch factors are suppressed. A Gaussian pulse model was adopted. The parameters are the following: the relative mismatch $\Delta = \tau - \tau'$; the attenuation factor due to time mismatch, f_0 [Eq. (11)]; and $C_0 = (a_L + a_S)/4$ [Eq. (12b)]:

$$s_{\sigma,0(1)} \propto \frac{1}{2}\left(\frac{\pi}{C_0}\right)^{1/2} f_0 F \sin\Phi_{0(2)},$$

$$s_{OR,0(1)} \propto \frac{1}{2}\frac{\pi}{\sqrt{a_L a_S}} f_0 F \exp\left[\frac{1}{2T_{OR}}\left(\tau + \tau' + \frac{1}{2C_{OR}T_{OR}}\right) - \frac{C_{OR}}{4}\Delta^2\right]\sin\Phi_{0(2)} \times \operatorname{erfc}\{[1/T_{OR} + C_{OR}(\tau + \tau')]/2\sqrt{C_{OR}}\},$$

$$s_{R,0} \propto -\frac{\pi}{4C_0} f_0 \exp\left\{-\frac{t_D}{T_2}\right\}\exp\left[\frac{1}{4C_0T_2}\left(a_L\Delta + \frac{1}{T_2}\right)\right] \times \cos\Phi_0 \operatorname{erfc}[-(C_0 t_D + B_0^-)/\sqrt{C_0}],$$

$$s_{R,1} \propto -\frac{\pi}{4C_0} f_0 \exp\left\{\frac{1}{4C_0}\left[\frac{1}{T_2}\left(a_L(\Delta - t_D) + \frac{1}{T_2}\right) + a_L a_S t_D\left(\tau - \frac{t_D}{2}\right)\right]\right\}\cos\Phi_1 \times \operatorname{erfc}[-(a_L t_D/4 - B_0^-)/\sqrt{C_0}],$$

$$s_{R,2} \propto -\frac{\pi}{4C_0} f_0 \exp\left(\frac{1}{4C_0}\left\{\frac{1}{T_2}\left[-a_L\Delta + \frac{1}{T_2} + (a_L - a_S)t_D\right] + a_L a_S t_D(\Delta - t_D)\right\}\right)\cos\Phi_2 \times \operatorname{erfc}\{[(a_L - a_S)t_D/4 - B_0^+]/\sqrt{C_0}\},$$

$$s_{R,3} \propto -\frac{\pi}{4C_0} f_0 \exp\left(\frac{1}{4C_0}\left\{\frac{1}{T_2}\left[a_L(t_D - \Delta) + \frac{1}{T_2}\right] + a_L a_S t_D\left(\tau - \frac{t_D}{2}\right)\right\}\right)\cos\Phi_1 \times \operatorname{erfc}[(a_L t_D/4 - B_0^+)/\sqrt{C_0}],$$

with

$$\Phi_0 = \phi_{L'} - \phi_{S'} - (\phi_L - \phi_S) - \omega_L\Delta + (\omega_L - \omega_S)t_D,$$

$$\Phi_2 = -(\phi_{L'} + \phi_{S'}) + (\phi_L + \phi_S) + \omega_L\Delta - (\omega_L + \omega_S)t_D,$$

$$\Phi_1 = \phi_{L'} - \phi_L - \omega_L\Delta + \omega_L t_D,$$

$$F = \exp[-(a_L\Delta - 4C_0 t_D)^2/(16C_0)],$$

$$B_0^{\mp} = -\frac{1}{2T_2} \mp \frac{a_L}{4}\Delta.$$

APPENDIX C: ANALYTICAL EXPRESSIONS FOR THE DEPHASING SIGNAL INCLUDING THE DOMAIN MODEL

The following expressions for the various TR SRG contributions were obtained according to the domain model for the laser pulses, with fixed values of δ_L, δ_S, and Γ. $w(z)$ is the complex error function, defined as $w(z) = \exp(-z^2)\operatorname{erfc}(-iz)$:

$$s_{\sigma,0} \propto \sigma m_0\left(\frac{\pi}{4C_0}\right)^{1/2} f_\Gamma F F_\beta^- \sin(\Phi_0 + R_{\beta,0} + 2Q_{\beta,0}t_D),$$

$$s_{\sigma,1} \propto \sigma m_2\left(\frac{\pi}{4C_0}\right)^{1/2} f_\Gamma F F_\beta^+ \sin(\Phi_2 + R_{\beta,2} + 2Q_{\beta,2}t_D),$$

$$s_{OR,0}^{\mp} \propto \frac{d_{OR}}{T_{OR}} m_0 \frac{\pi}{2\sqrt{a_L a_S}} f_\Gamma F F_\beta^{-1/2} \times \sin\{\Phi_0 + R_{\beta,0} + 2Q_{\beta,0}t_D - \arg[w(Z_\mp)]\}\operatorname{mod}[w(Z_\mp)],$$

with

$$Z_\mp = -i(C_{OR}t_D + B_{0,\Gamma} \pm i\Omega_{OR}/2)/\sqrt{C_{OR}} + Q_\beta^-/\sqrt{C_{OR}};$$

$$s_{OR,1}^{\mp} \propto \frac{d_{OR}}{T_{OR}} m_2 \frac{\pi}{2\sqrt{a_L a_S}} f_\Gamma F F_\beta^{+1/2} \times \sin\{\Phi_2 + R_{\beta,2} + 2Q_{\beta,2}t_D - \arg[w(Z_\mp)]\}\operatorname{mod}[w(Z_\mp)],$$

with

$$Z_\mp = -i(C_{OR}t_D + B_{0,\Gamma} \pm i\Omega_{OR}/2)/\sqrt{C_{OR}} + Q_\beta^+/\sqrt{C_{OR}};$$

$$s_{R,0} \propto -\frac{d_R}{2T_2} m_0 \frac{\pi}{4\sqrt{C_0 C_\beta}} f_\Gamma F F_\beta^- \times \cos\{\Phi_0 + R_{\beta,0} + 2Q_{\beta,0}t_D - \arg[w(Z)]\}\operatorname{mod}[w(Z)],$$

with

$$Z = -i[C_\beta t_D + B_0^- - i\delta_R/2 + i(\delta_L - \delta_S)/2]/\sqrt{C_\beta} - i(B_{\beta,0} + iQ_{\beta,0})/\sqrt{C_\beta};$$

$$s_{R,1} \propto -\frac{d_R}{2T_2} m_1 \frac{\pi}{4\sqrt{C_0 C_\beta}} f_\Gamma F F_\beta' F_\Gamma \times \cos\{\Phi_1 + R_{\beta,1} - \arg[w(Z)]\}\operatorname{mod}[w(Z)],$$

with

$$Z = -i[a_L/(4t_D) + B_0^- - i\delta_R/2 + i(\delta_L - \delta_S)/2]/\sqrt{C_\beta} - i(B_{\beta,1} + iQ_{\beta,1})/\sqrt{C_\beta};$$

$$s_{R,2} \propto -\frac{d_R}{2T_2} m_2 \frac{\pi}{4\sqrt{C_0 C_\beta}} f_\Gamma F F_\beta^+ \times \cos\{\Phi_2 + R_{\beta,2} + 2Q_{\beta,2}t_D - \arg[w(Z)]\}\operatorname{mod}[w(Z)],$$

with

$$Z = -i[C_\beta t_D + B_2 - i\delta_R/2 + i(\delta_L - \delta_S)/2]/\sqrt{C_\beta} - i(B_{\beta,2} + iQ_{\beta,2})/\sqrt{C_\beta};$$

$$s_{R,3} \propto -\frac{d_R}{2T_2} m_1 \frac{\pi}{4\sqrt{C_0 C_\beta}} f_\Gamma F F_\beta' F_\Gamma \times \cos\{\Phi_1 + R_{\beta,1} + \arg[w(Z)]\}\operatorname{mod}[w(Z)],$$

with

$$Z = -i[-a_L t_D/4 + B_0^+ - i\delta_R/2 + i(\delta_L - \delta_S)/2]/\sqrt{C_\beta} - i(-B_{\beta,1} + iQ_{\beta,1})/\sqrt{C_\beta}.$$

The following notation is used in the text and in Fig. 3:

$$s_{\mathrm{OR},0(1)} = s^{-}_{\mathrm{OR},0(1)} + s^{+}_{\mathrm{OR},0(1)},$$

$$s^{\mathrm{eff}}_{\mathrm{OR},0} = \{(s^{-}_{\mathrm{OR},0})^2 + (s^{+}_{\mathrm{OR},0})^2 + 2s^{-}_{\mathrm{OR},0}s^{+}_{\mathrm{OR},0}\cos[(\arg(s^{-}_{\mathrm{OR},0}) - \arg(s^{+}_{\mathrm{OR},0})]\}^{1/2},$$

with an analogous expression for $s^{\mathrm{eff}}_{\mathrm{OR},1}$.

Unless explicitly marked, all the following parameters X are $X \equiv X[\tau, \tau'(\Gamma)(t_D)]$:

$$F = \exp[-(a_L\Delta - 4C_0t_D)^2/(16C_0)],$$

$$F_\Gamma = \exp\left[\frac{t_D}{2}\left(\frac{a_S}{2a_L}C_{\mathrm{OR}}t_D + C_\Gamma\right)\right],$$

$$F'_\beta = \exp\{-[a_L\beta_L(\Delta - t_D)]^2/(16C_0)\},$$

$$F^{\mp}_\beta = \exp\{-[a_L\beta_L\Delta - (a_L\beta_L \mp a_S\beta_S)t_D]^2/(16C_0)\},$$

$$f_\Gamma = \exp\{-C_{\mathrm{OR}}[(\tau + \Gamma)^2 + (\tau' + \Gamma)^2]/2\}.$$

In the above formulas the symbols have the following meanings:

$$\Delta = \tau - \tau',$$

$$C_0 = (a_L + a_S)/4,$$

$$C'_\beta = (a_L\beta_L - a_S\beta_S)/(a_L + a_S),$$

$$C_\beta = C_0(1 + C'^2_\beta),$$

$$C_{\mathrm{OR}} = a_La_S/(a_L + a_S),$$

$$C_\Gamma = C_{\mathrm{OR}}(\tau + \tau' + 2\Gamma),$$

$$B_{0,\Gamma} = -(1/T_{\mathrm{OR}} + C_\Gamma + 2C_{\mathrm{OR}}t_D)/2,$$

$$B^{\mp}_0 = -\frac{1}{2T_2} \mp \frac{a_L}{4}\Delta,$$

$$B_2 = B^{+}_0 - a_Lt_D/2,$$

$$B_{\beta,0} = -a_L\beta_LC'_\beta\Delta/4,$$

$$B_{\beta,1}(\tau, \tau') = B_{\beta,0}(\Delta - t_D),$$

$$B_{\beta,2} = a_L\beta_LC'_\beta(\Delta - 2t_D)/4,$$

$$Q^{\mp}_\beta = \mp C_{\mathrm{OR}}[(\beta_L \pm \beta_S)t_D - \beta_L\Delta]/2,$$

$$Q_{\beta,0} = (\beta_L + \beta_S)C_\Gamma/4,$$

$$Q_{\beta,1}(\tau, \tau', \Gamma) = Q_{\beta,0}(\tau - t_D, \tau', \Gamma),$$

$$Q_{\beta,2} = Q_{\beta,0},$$

$$R_{\beta,0} = -C_\Gamma\beta_L\Delta/2,$$

$$R_{\beta,1} = -\beta_L\{C_{\mathrm{OR}}t_D[t_D - 2(\tau + \Gamma)] + C_\Gamma\Delta\}/2,$$

$$R_{\beta,2} = C_\Gamma\beta_L(\Delta - 2t_D)/2,$$

$$R_{\beta,i} + 2Q_{\beta,i}t_D = C_\Gamma[(\beta_L + \beta_S)t_D - \beta_L\Delta]/2 \quad \text{for } i = 0,$$

$$= -C_\Gamma[(\beta_L - \beta_S)t_D - \beta_L\Delta]/2 \quad \text{for } i = 2.$$

Φ_0, Φ_1, and Φ_2 are the same as in Appendix B, provided that $(\omega_L + \delta_L)$ is substituted for ω_L and $(\omega_S + \delta_S)$ for ω_S:

$$\Phi_0 = \phi_{L'} - \phi_{S'} - \phi_L + \phi_S - \omega_L\Delta + (\omega_L - \omega_S)t_D - \delta_L\Delta + (\delta_L - \delta_S)t_D,$$

$$\Phi_1 = \phi_{L'} - \phi_L - \omega_L\Delta + \omega_Lt_D - \delta_L\Delta + \delta_Lt_D,$$

$$\Phi_2 = -\phi_{L'} - \phi_{S'} + \phi_L + \phi_S + \omega_L\Delta - (\omega_L + \omega_S)t_D + \delta_L\Delta - (\delta_L + \delta_S)t_D.$$

It should be recalled that ϕ_L carries the applied phase modulations (Subsection 3.A).

Finally, for our specific geometry the mismatch factors m_i are

$$m_0 = 0.89,$$

$$m_1 = 4.3 \times 10^{-2},$$

$$m_2 = 1.71 \times 10^{-2}.$$

ACKNOWLEDGMENTS

The authors thank A. Bouwen for his experimental and logistic support and P. Casteels for automating the equipment. This research was supported by the Geconcerteerde Acties (Ministerie van Wetenschapsbeleid) and the Interuniversitair Instituut voor Kernwetenschappen, to which the authors are greatly indebted. M. De Mazière thanks the National Fund for Scientific Research for a research assistantship.

* Present address, Belgian Institute for Space Aeronomy, Ringlaan 3, B-1180, Brussels, Belgium.

† Present address, ALCATEL-Bell Telephone Company, F. Wellesplein 1, B-2018 Antwerp, Belgium.

REFERENCES

1. D. Von Der Linde, in *Ultrashort Light Pulses*, S. L. Shapiro, ed. (Springer-Verlag, Berlin, 1978).
2. M. J. Burns, W. K. Liu, and A. H. Zewail, in *Spectroscopy and Excitation Dynamics of Condensed Molecular Systems*, V. M. Agranovich and R. M. Hochstrasser, eds. (North-Holland, Amsterdam, 1983), p. 301.
3. W. H. Hesselink and D. A. Wiersma, in *Spectroscopy and Excitation Dynamics of Condensed Molecular Systems*, V. M. Agranovich and R. M. Hochstrasser, eds. (North-Holland, Amsterdam, 1983), p. 249.
4. M. D. Levenson, *Introduction to Nonlinear Laser Spectroscopy* (Academic, New York, 1982).
5. A. Penzkofer, A. Laubereau, and W. Kaiser, Prog. Quantum Electron. **6**, 55 (1979).
6. A. Laubereau and W. Kaiser, Rev. Mod. Phys. **50**, 607 (1978).
7. S. Velsko and R. M. Hochstrasser, J. Phys. Chem. **89**, 2240 (1985).
8. C. H. Lee and D. Ricard, Appl. Phys. Lett. **32**, 168 (1978).
9. J. P. Heritage, Appl. Phys. Lett. **34**, 470 (1979).
10. J.-L. Oudar, IEEE J. Quantum Electron. **QE-19**, 713 (1983).
11. M. Van Exter and A. Lagendijk, Opt. Commun. **56**, 191 (1985).
12. R. M. Hochstrasser, G. R. Meredith, and H. P. Trommsdorff, J. Chem. Phys. **73**, 1009 (1980); P. L. Decola, R. M. Hochstrasser, and H. P. Trommsdorff, Chem. Phys. Lett. **72**, 1 (1980); D. D. Dlott, C. L. Schosser, and E. L. Chronister, Chem. Phys. Lett. **90**, 386 (1982); S. Velsko, J. Trout, and R. M. Hochstrasser, J. Chem. Phys. **79**, 2114 (1983).
13. R. L. St. Peters, Opt. Lett. **4**, 401 (1979).

14. R. H. Picard and P. Schweitzer, Phys. Rev. A **1,** 1803 (1970).
15. M. De Mazière, A. Bouwen, and D. Schoemaker, J. Opt. Soc. Am. B **6,** 2370 (1989).
16. M. De Mazière and D. Schoemaker, J. Appl. Phys. **58,** 1439 (1985).
17. M. De Mazière, Ph.D. dissertation (University of Antwerp, Antwerp, Belgium, 1986).
18. J. Kluge, D. Wiechert, and D. Von der Linde, Opt. Commun. **51,** 271 (1984).
19. R. W. Hellwarth, Prog. Quantum Electron. **5,** 1 (1977).
20. H. Lotem and R. T. Lynch, Jr., Phys. Rev. Lett. **37,** 334 (1976).
21. H. Lotem, R. T. Lynch, Jr., and N. Bloembergen, Phys. Rev. A **14,** 1748 (1976).
22. J. J. Song and M. D. Levenson, J. Appl. Phys. **48,** 3496 (1977).
23. M. D. Levenson and N. Bloembergen, J. Chem. Phys. **60,** 1323 (1974).
24. S. L. Shapiro and H. P. Broida, Phys. Rev. **154,** 129 (1967); M. A. F. Scarparo, J. H. Lee, and J. J. Song, Opt. Lett. **6,** 193 (1981); J. Etchepare, G. A. Kenney-Wallace, G. Grillon, A. Migus, and J. P. Chambaret, IEEE J. Quantum Electron **QE-18,** 1826 (1982).
25. J. Etchepare, G. Grillon, R. Astier, J. L. Martin, C. Bruneau, and A. Antonetti, in *Picosecond Phenomena III,* K. B. Eisenthal, R. M. Hochstrasser, W. Kaiser, and A. Laubereau, eds. (Springer-Verlag, New York, 1982), p. 217.
26. G. J. Rosasco, W. S. Hurst, and W. Lempert, Opt. Lett. **9,** 19 (1984).
27. A. J. Duerinckx, H. B. Vanherzeele, J. L. Van Eck, and A. E. Siegman, IEEE J. Quantum Electron. **QE-14,** 983 (1978).
28. S. Asaka, H. Nakatsuka, M. Fujiwara, and M. Matsuoka, Phys. Rev. A **29,** 2286 (1984); N. Morita and T. Yajima, Phys. Rev. A **30,** 2525 (1984).
29. H. J. Eichler, D. Langhans, and F. Massmann, Opt. Commun. **50,** 117 (1984).
30. B. Wilhelmi and J. Herrmann, Sov. J. Quantum Electron. **10,** 1082 (1980).
31. A. von Jena and H. E. Lessing, Appl. Phys. B **19,** 131 (1979); A. von Jena, Appl. Phys. **26,** 1 (1981).
32. Z. Vardeny and J. Tauc, Opt. Commun. **39,** 396 (1981).
33. T. F. Heinz, S. L. Palfrey, and K. B. Eisenthal, Opt. Lett. **9,** 359 (1984).
34. W. M. Tolles, J. W. Nibler, J. R. McDonald, and A. B. Harvey, Appl. Spectrosc. **31,** 253 (1977).
35. B. K. Rhee, W. E. Bron, and J. Kuhl, Phys. Rev. B **30,** 7358 (1984); J. Kuhl and W. E. Bron, Solid State Commun. **49,** 935 (1984).
36. F. M. Kamga and M. G. Sceats, Opt. Lett. **5,** 126 (1980); F. M. Kamga, Ph.D. dissertation (University of Rochester, Rochester, N.Y., 1979).
37. W. Zinth, Opt. Commun. **34,** 479 (1980); W. Zinth, A. Laubereau, and W. Kaiser, Opt. Commun. **26,** 457 (1978).
38. J. Eggleston and R. L. Byer, IEEE J. Quantum Electron. **QE-16,** 850 (1980).
39. J. E. Golub and T. W. Mossberg, Opt. Lett. **11,** 431 (1986).
40. A. Laubereau, G. Wochner, and W. Kaiser, Phys. Rev. A **13,** 2212 (1976).
41. C. Sierens, A. Bouwen, E. Goovaerts, M. De Mazière, and D. Schoemaker, Phys. Rev. A **37,** 4769 (1988).
42. B. F. Levine, C. V. Shank, and J. P. Heritage, IEEE J. Quantum Electron. **QE-15,** 1418 (1979).